Chemical Science

ROYAL SOCIETY OF CHEMISTRY

EDGE ARTICLE

View Article Online
View Journal | View Issue

Cite this: *Chem. Sci.*, 2021, **12**, 2114

All publication charges for this article have been paid for by the Royal Society of Chemistry

Received 15th September 2020
Accepted 4th December 2020

DOI: 10.1039/d0sc05108j

rsc.li/chemical-science

Ultrafast structural dynamics of in-cage isomerization of diiodomethane in solution†

Hanui Kim,[abc] Jong Goo Kim,[c] Tae Wu Kim, ‡[c] Sang Jin Lee,[abc] Shunsuke Nozawa,[de] Shin-ichi Adachi,[de] Kihwan Yoon,[f] Joonghan Kim [f] and Hyotcherl Ihee *[abc]

Despite extensive studies on the isomer species formed by photodissociation of haloalkanes in solution, the molecular structure of the precursor of the isomer, which is often assumed to be a vibrationally hot isomer formed from the radical pair, and its in-cage isomerization mechanism remain elusive. Here, the structural dynamics of CH_2I_2 upon 267 nm photoexcitation in methanol were probed with femtosecond X-ray solution scattering at an X-ray free-electron laser. The determined molecular structure of the transiently formed species that converts to the CH_2I–I isomer has the I–I distance of 4.17 Å, which is longer than that of the isomer (3.15 Å) by more than 1.0 Å and the mean-squared displacement of 0.45 $Å^2$, which is about 100 times larger than those of typical regular chemical bonds. These unusual structural characteristics are consistent with either a vibrationally hot form of the CH_2I–I isomer or the loosely-bound radical pair ($CH_2I^{\bullet}\cdots I^{\bullet}$).

Introduction

The solvent cage[1,2] plays various roles in chemical dynamics by influencing the energy landscape of reacting species, altering the reaction rates, and even changing the reaction pathways.[3–12] For example, the primary products of photodissociation, which are completely separated in the gas phase, collide with the surrounding solvent molecules and can be trapped in the solvent cage upon failure to escape the cage.[1,2] A typical fate of the trapped photofragments is to undergo geminate recombination, a ubiquitous process in the solution phase, which generally leads the transient species to the initial ground state. In the case of haloalkanes, geminate recombination can yield an isomer species as well as the parent molecule.[13–17] Since the formation of the isomer is rarely observed in the gas phase,[18–21] the chemical dynamics of the isomer formation has been an important topic of many experimental investigations to understand the role of the solvent cage. In this regard, diiodomethane, CH_2I_2, is a prototypical example and its photodissociation is known to produce a unique isomer

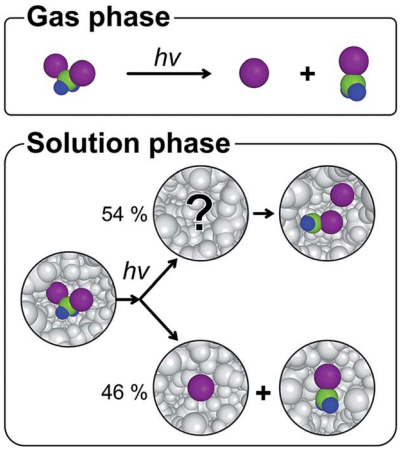

Fig. 1 The photodissociation dynamics of CH_2I_2 in the gas and solution phases. Whereas the products in the gas phase are $CH_2I^{\bullet}$ and $I^{\bullet}$ radicals ($CH_2I^{\bullet} + I^{\bullet}$), the CH_2I–I isomer is also observed in the solution phase. The green, blue and purple balls indicate carbon, hydrogen, and iodine atoms, respectively. Whereas the branching ratio into the CH_2I–I isomer and $CH_2I^{\bullet} + I^{\bullet}$ of 54 : 46 and the molecular structure of the CH_2I–I isomer were determined in a previous TRXL study at a synchrotron, the exact structure of the precursor of the stable CH_2I–I isomer remained to be determined and was probed with femtosecond TRXL in this study.

[a]Department of Chemistry, Korea Advanced Institute of Science and Technology (KAIST), Daejeon 34141, Republic of Korea. E-mail: hyotcherl.ihee@kaist.ac.kr
[b]KI for the BioCentury, Korea Advanced Institute of Science and Technology (KAIST), Daejeon 34141, Republic of Korea
[c]Center for Nanomaterials and Chemical Reactions, Institute for Basic Science (IBS), Daejeon 34141, Republic of Korea
[d]Photon Factory, Institute of Materials Structure Science, High Energy Accelerator Research Organization (KEK), Tsukuba, Ibaraki 305-0801, Japan
[e]Department of Materials Structure Science, School of High Energy Accelerator Science, The Graduate University for Advanced Studies, Tsukuba, Ibaraki 305-0801, Japan
[f]Department of Chemistry, The Catholic University of Korea, Bucheon 14662, Republic of Korea

† Electronic supplementary information (ESI) available. See DOI: 10.1039/d0sc05108j

‡ Present address: Chemical Sciences and Engineering Division, Argonne National Laboratory, Lemont, Illinois 60439, United States.

species, isodiiodomethane (CH_2I–I),[22–34] which has no analog in the gas phase (Fig. 1).[19,35–37]

The photodissociation dynamics of CH_2I_2 and the formation of CH_2I–I isomer in solution have been mainly investigated with ultrafast transient absorption (TA) spectroscopy[22–24,38,39] and transient resonance Raman (TRR) spectroscopy,[25–28] which successfully identified the transient spectrum assigned to the isomer and the time scale of the isomer formation. As UV excitation of CH_2I_2 induces the n(I) → σ*(C–I) transition, one of the two C–I bonds in CH_2I_2 dissociates. The studies using TA spectroscopy uncovered that the excited molecule rapidly dissociates into $CH_2I^{\bullet}$ and $I^{\bullet}$ fragments and recombines to form the CH_2I–I isomer with a time constant of ∼5 ps.[22–24] It is also known that a part of $I^{\bullet}$ radicals escape the solvent cage and form $CH_2I^{\bullet}$ + $I^{\bullet}$ within about 120 fs.[38,39] Here $CH_2I^{\bullet}$ + $I^{\bullet}$ denotes the $CH_2I^{\bullet}$ and $I^{\bullet}$ photofragments that are completely separated and not in the same solvent cage. The TRR study suggested that the vibrationally hot CH_2I–I isomer is initially formed upon UV excitation with the time scale of a few ps and then subsequently undergoes vibrational cooling on the 4–50 ps time scale.[25–28] Based on their results, it was suggested that the solvation leads to the isomer *via* the interaction of the initially photolyzed $CH_2I^{\bullet}$ and $I^{\bullet}$ radicals with the solvent cage. Nevertheless, the structural nature of the hot isomer, the precursor of the cold CH_2I–I isomer, still remains unanswered. The detailed mechanism of the isomer formation and the structure of the hot isomer or the radical pair have been elusive and only speculated from indirect evidence. In this regard, the photodissociation dynamics of CH_2I_2 in solution was studied also by time-resolved X-ray liquidography (TRXL), also known as time-resolved X-ray solution scattering, which is an effective method for probing photoinduced structural changes of molecules in solution due to the structural sensitivity of X-ray scattering.[7,40–42] The TRXL studies accurately identified the structure of the CH_2I–I isomer,[29,30] determined its fate at later times,[31] and revealed that the photo-dissociated CH_2I_2 branches into the CH_2I–I isomer and $CH_2I^{\bullet}$ + $I^{\bullet}$ radical pathways with the 54 : 46 ratio.[31] Nevertheless, since the temporal resolution of TRXL based on the synchrotron radiation was limited to ∼100 ps, the mechanism of isomer formation, which occurs at a few picosecond time scale, could not be investigated. With the advent of X-ray free electron lasers (XFELs),[43–48] TRXL with femtosecond time resolution has become possible.[49–56] In this article, we employed femtosecond TRXL on CH_2I_2 with 267 nm excitation to study the formation mechanism of the CH_2I–I isomer with direct structural information. The structure of the isomer precursor is unveiled by the structural fitting analysis and also complemented by the quantum chemical calculations.

Experimental

The femtosecond TRXL experiment performed in this study is shown schematically in Fig. S1,† and the details of the experimental and analysis procedures are described in the ESI.† Briefly, a CH_2I_2 solution in methanol at the concentration of 50 mM was circulated through a sapphire nozzle with a 100 μm-thick aperture. A 100 fs laser pulse with the center wavelength of 267 nm generated by third-harmonic generation of the 800 nm femtosecond laser and with the fluence of 1 mJ mm^{-2} initiates the photodissociation of CH_2I_2 molecule. A time-delayed X-ray pulse with the center energy of 15 keV generated at the BL3 beamline of SACLA probes the progress of the reaction. The scattering patterns generated by X-ray pulses were measured with an area detector (Rayonix LX255-HS). Each scattering image was obtained by accumulating scattering intensities of 40 X-ray pulses, which provided a sufficient signal to noise ratio and suppressed the effect from jitter of the SASE process at SACLA. The difference scattering patterns were generated by subtracting the reference images which were acquired at −20 ps. The time-dependent changes were measured at various time delays ranging from −10 ps to 100 ps. By performing the singular value decomposition (SVD) analysis and kinetic analysis on our experimental data, two species-associated difference scattering curves (SADSs) and one time constant were obtained. The structural changes were extracted by the structural fitting analysis of the SADSs. The theoretical characterization of $CH_2I^{\bullet}\cdots I^{\bullet}$ in the solvent cage using CCSD(T) is described in the ESI.†

Results and discussion

The experimental difference scattering curves were measured at various time delays from −10 ps to 100 ps, and those at selected time delays are shown in Fig. 2a. From the SVD analysis on the data and the subsequent kinetic analysis by solving the rate equations and convoluting with the instrument response

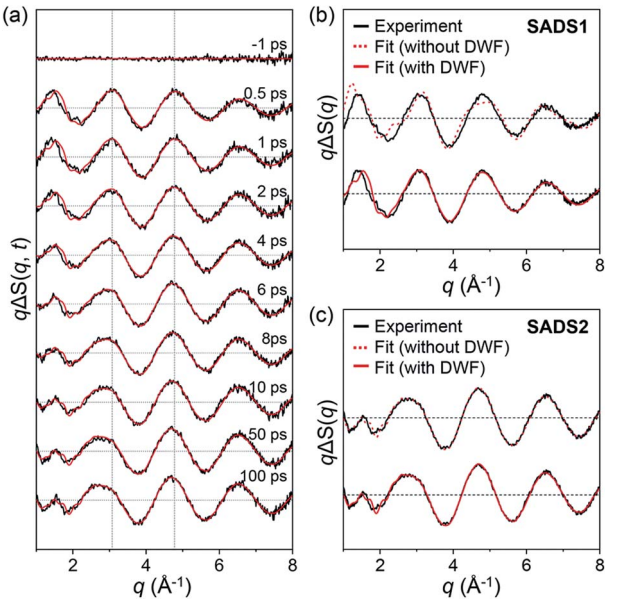

Fig. 2 (a) Experimental difference scattering curves, $q\Delta S(q)$, measured at various time delays from −1 ps to 100 ps (black) and calculated $q\Delta S(q)$ (red) to fit the experimental curves. For clarity, data at selected time delays instead of all time delays are shown. (b and c) The structural fitting analysis of (b) SADS1 and (c) SADS2. The SADSs (black, solid line) are compared with the fitted curves without (top, red dashed line) and with (bottom, red solid line) introducing a DWF for the I–I distance.

function (IRF), as described in the ESI,† we obtained two SADSs shown in Fig. 2b and c and a single time constant of 6.2 ± 0.8 ps for the conversion from the first species to the second species with an IRF of 540 ± 90 fs full-width at half-maximum. We termed the first and second SADSs as SADS1 and SADS2, respectively. We first checked if SADS2 was consistent with the previous data, the curve at 150 ps measured at a synchrotron. A comparison confirms that they are identical within the experimental errors as shown in Fig. S5.† According to the previous TRXL study,[31] 23% of ground-state CH_2I_2 is initially photoexcited, and then 56.5% of the excited molecules directly relax back to the ground state, releasing a part of the photoexcitation energy as heat to surrounding solvent molecules. The remaining 43.5% of excited molecules form CH_2I–I isomer and $CH_2I^{\bullet}$ + $I^{\bullet}$ with the branching ratio of 54 : 46. When SADS2 is fitted with the fraction and I–I distance (R_{I-I}) of CH_2I–I isomer as fitting parameters, the best fit yielded 53.9 ± 5.2% and 3.15 ± 0.02 Å, which are consistent with 54% and 3.15 Å reported in a previous study,[31] and the theoretical difference scattering curve gives an excellent agreement with SADS2 as shown in Fig. 2c. This result means that the CH_2I–I isomer and $CH_2I^{\bullet}$ + $I^{\bullet}$ are formed with a time constant of 6.2 ps *via* the conversion from the species generated at the onset of the reaction. Accordingly, the time constant must be responsible for the formation of either the CH_2I–I isomer or $CH_2I^{\bullet}$ + $I^{\bullet}$. Among these two possibilities, it is highly likely that the isomer is formed with the observed time constant of 6.2 ps because 6.2 ps agrees well with the values (5 ps in TA,[22–24] 4–50 ps time scales in TRR[25–28]) reported for the isomer formation in the previous spectroscopic studies.

From the TA and TRR studies, it was suggested that the cold CH_2I–I isomer is formed by the vibrational cooling of the hot CH_2I–I isomer.[22–28] However, since the spectroscopic signals at the optical frequencies are not directly related to the global molecular structures at the atomic level, the structure of the hot isomer, or the precursor of the cold isomer, remains to be determined. SADS1 contains the structural information necessary for this purpose, and to shed light on the identity of the precursor of the isomer, we performed the structural fitting analysis of SADS1. The detailed analysis protocol is described in our previous publications[31] and also in the ESI.† To describe the relatively free movement of the weakly bound I atom, we incorporated a Debye–Waller factor (DWF),[57,58] $\exp(-\sigma^2 q^2/2)$, involving the mean-squared displacement (σ^2) for R_{I-I} into the equation for calculating the theoretical scattering pattern (see the ESI† for details). We note that for a typical analysis of TRXL data, DWF of 1 (that is, $\sigma^2 = 0$) used for all interatomic distances suffices unless the interatomic distance has an unusually large σ^2.

The fitting results summarized in Fig. 2b show that the theoretical SADS1 agrees well with the experimental SADS1 when a DWF is considered (Fig. 2b, red solid line). The best fit gives R_{I-I} of 4.17 Å and σ^2 of 0.45 Å^2. The R_{I-I} of 4.17 Å is longer than that of the isomer (3.15 Å) by more than 1.0 Å, and the σ^2 value of 0.45 Å^2 is about 100 times larger than that of typical regular chemical bonds (for example, 4.9 × 10^{-3} Å^2 for R_{I-I} in I_3^-).[59] Such a long R_{I-I} and an unusually large σ^2 are consistent with a picture expected for the precursor of isomer as either the hot isomer or the loosely-bound radical pair in the cage. For a fair comparison, we performed the structural fitting analysis on SADS2 again with a DWF. As shown in Fig. 2c, the fit curve shows no noticeable change compared to the one calculated without using a DWF, and a typical small σ^2 value (smaller than 1.2 × 10^{-3} Å^2) was obtained, confirming that the CH_2I–I isomer formed at later delays has a well-defined R_{I-I}. To check the sensitivity of SADS1 to the structural parameters, we scanned the chi-square values as a function of both R_{I-I} and σ^2 of the precursor of isomer. The relative chi-square values, which are the chi-square values divided by the minimum chi-square value of SADS1, are displayed in Fig. 3a. Fig. 3a shows that the fit quality is comparable for a wide range of R_{I-I} from 3.9 Å to 4.4 Å rather than a single well-defined value. For comparison, we performed the same analysis on SADS2 and obtained the relative chi-square values as a function of R_{I-I} and σ^2 of the cold isomer, which shows well-defined values contrary to the precursor of isomer (Fig. 3b). In Fig. 3a and b, the C–I–I angle was fixed at that of the optimized structure, 79.4° and 115° for the loosely-bound isomer precursor (Fig. 3a) and the CH_2I–I isomer (Fig. 3b), respectively.

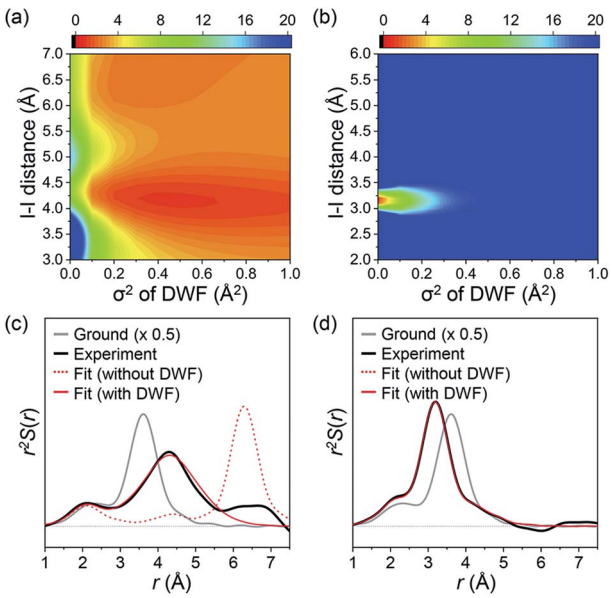

Fig. 3 (a and b) Plots of the relative chi-square values of (a) SADS1 and (b) SADS2 as a function of the I–I distance (R_{I-I}) and the mean-squared displacement (σ^2) of (a) the loosely-bound isomer precursor and (b) the CH_2I–I isomer. The loosely-bound isomer precursor has the minimum at R_{I-I} = 4.2 Å and σ^2 = 0.5 Å^2 with large widths whereas the CH_2I–I isomer has the minimum at R_{I-I} = 3.2 Å and σ^2 = 0.0 Å^2 with sharp widths. (c and d) Two experimental species-associated RDFs, $r^2S(r)$, obtained by Fourier sine transformation of (c) SADS1 and (d) SADS2, after subtracting solvent and cage contributions. The RDF of the ground state (CH_2I_2) was added to the difference RDFs, to emphasize the contributions of the transient solute species. The experimental species-associated RDFs are compared with the RDF of the ground state CH_2I_2 (gray solid line, multiplied by 0.5) and the RDFs obtained from the structural fitting analysis of (c) SADS1 and (d) SADS2 with (red solid line) and without (red, dashed line) introducing a DWF for the I–I distance.

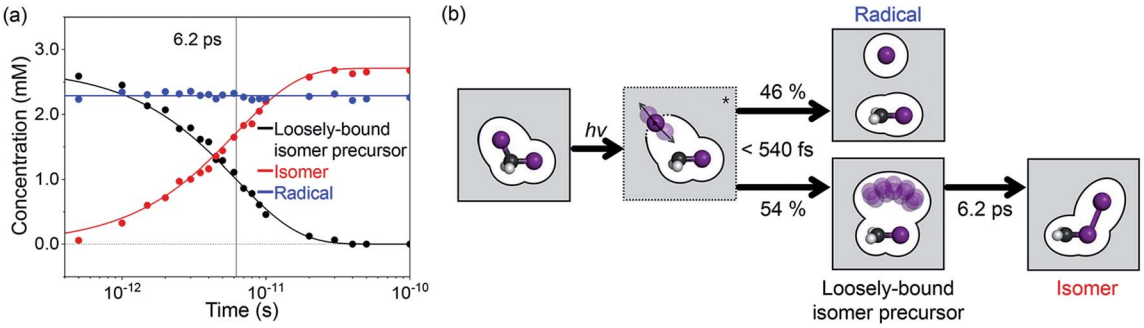

Fig. 4 (a) Time-dependent concentrations of the three intermediate species and their transition kinetics. The black, red, and blue indicate the isomer precursor in the cage, the isomer (CH_2I–I), and the radical ($CH_2I^{\bullet}$ + $I^{\bullet}$), respectively. The lines are the concentrations obtained from the kinetics analysis. Dots represent the optimized concentrations calculated from the coefficients of SADSs obtained by fitting the experimental curve at each time point with a linear combination of SADSs. The vertical black line indicates the temporal position of the time constant of 6.2 ps. (b) Mechanism of photoinduced in-cage isomerization in CH_2I_2. Upon photoexcitation of CH_2I_2, the dissociated iodine atom initially moves away from the carbon atom and the solvent molecules disturb the separation. Within our time resolution (~540 fs), 46% of the dissociated iodine escapes from the solvent cage ($CH_2I^{\bullet}$ + $I^{\bullet}$), and 54% of the dissociated iodine is blocked by solvent molecules and forms the loosely-bound isomer precursor inside of the cage. The elongated R_{I-I} (4.27 Å) and the Debye–Waller factor with a high mean-squared displacement (0.45 $Å^2$) indicate that the isomer precursor in the cage is loosely bound and does not have a well-defined R_{I-I}. Subsequently, it transforms into the CH_2I–I isomer species with a time scale of 6.2 ps.

A more intuitive picture of the structural changes that occur during the photodissociation and in-cage isomerization of CH_2I_2 can be obtained when we convert SADSs into the species-associated radial distribution functions (RDFs) in real space by Fourier sine transformation (Fig. 3c and d). To emphasize only the contributions of transient solute species, we subtracted the contributions from the solvent heating and solvent–solute cross term. We also added the RDF of the ground state (CH_2I_2) to the difference RDFs. Because all the solvent contributions are eliminated and the scattering from C and H atoms is much smaller compared to the scattering from I atoms, the RDFs shown in Fig. 3c and d mainly represent the interatomic distance between two iodine atoms and the contributions from C–I pairs are shown as a small shoulder at around 2.5 Å.

In the ground state, the peak corresponding to R_{I-I} is at 3.58 Å as shown in the gray solid line in Fig. 3c and d. Right after the laser excitation, the RDF exhibits three distinct changes as shown in the black solid line in Fig. 3c. First, the amplitude of the peak becomes much smaller than that of the ground state since about half of the population goes into $CH_2I^{\bullet}$ + $I^{\bullet}$, which has no I–I pair with a short enough R_{I-I} visible in the RDF. Second, the I–I peak is shifted to a longer distance (4.17 Å), indicating that the C–I bond is dissociated and the isomer precursor exists as a loosely-bound state within the solvent cage. Third, the I–I peak becomes much broader than that of the ground state, meaning that the isomer precursor is loosely bound and thus does not have a well-defined distance. This is fully consistent with the conclusion inferred from the results of the structural fitting analysis of SADS1. It is shown in Fig. 3c that the theoretical RDF with the DWF (red solid line) with σ^2 of 0.45 $Å^2$ fits well the experimental RDF while the one without DWF (red dashed line) does not. At later time delays, the I–I peak is shifted to the distance of 3.15 Å, which is even shorter than that of the ground state, and the width of the peak is also narrowed again, as shown in Fig. 3d. This indicates that there exists a well-defined I–I bond assignable to the CH_2I–I isomer formed at later time delays.

Finally, we analyzed all the experimental difference scattering curves measured at various time delays from 0.5 ps to 100 ps and all of them are well explained by the linear combinations of SADS1 and SADS2. The concentrations of each species at each time delay were determined from the coefficients of the corresponding SADSs as shown in Fig. 4a. The time-dependent changes of the concentration are then fitted with an exponential function and the time scale of the transition (6.2 ± 0.2 ps) agrees well with the one obtained from SVD analysis and also with the value reported in the previous spectroscopic studies.[22–28] In Fig. 4b, we summarize the mechanism for the photoinduced in-cage isomerization of CH_2I_2. Upon photoexcitation of CH_2I_2, the dissociated iodine atom initially moves away from the carbon atom and the solvent molecules disturb the separation. Within our time resolution (~540 fs), 46% of the dissociated iodine escapes from the solvent cage and generates $CH_2I^{\bullet}$ + $I^{\bullet}$ radical species, while the remaining 54% is blocked by solvent molecules and forms the loosely-bound precursor of the isomer inside of the solvent cage. Subsequently, the isomer precursor transforms into a rigid CH_2I–I isomer species with a time constant of 6.2 ps.

Since the TRXL signal itself is not sensitive to the spin state, the structural aspect of the isomer precursor alone does not pin down the exact nature of the isomer precursor, that is whether it is a hot isomer or a radical pair. Nevertheless, we further considered the possibility that the isomer precursor is indeed a radical pair. As a matter of fact, while the concept of the radical pair has been frequently discussed in the literature, the structural aspect has never been determined experimentally and has rarely been addressed in theoretical calculation. The theoretical characterization of the weakly bound molecule is not trivial because of the difficulty in describing the weak interaction and a significant non-dynamic electron correlation effect of

the singlet state molecule with a long bond length. *Via* performing CCSD(T)/AVTZ calculations, we found two molecular structures corresponding to radical pairs of the triplet state and they are consistent with the structure determined from our experiment (see the ESI† for details). The use of *ab initio* MD simulation with spin–orbit coupling in explicit solvent molecules would potentially be able to model the mechanism more accurately, but such an approach on a system with explicit solvent molecules is still challenging and beyond the scope of this work.

Conclusions

This work visualizes how the isomer is formed in the solvent cage *via* the loosely-bound isomer precursor, whose molecular structure remained to be determined, and provides structural information connecting chemical dynamics in the gas and liquid phases that were previously missing. This work also demonstrates that femtosecond TRXL offers a means of visualizing the entire process of photoinduced reactions in solution. Finally, we note that some other processes expected from the photodissociation dynamics of CH_2I_2 such as a rotational relaxation of the photofragments, the solvent cage rearrangement, and the escape dynamics of $I^\bullet$ radical are not significant in our data, probably due to the limited time resolution. Nevertheless, by fully utilizing the recent advances of the femtosecond TRXL,[52–56] future TRXL studies with improved time resolutions will surely reveal structural details of such processes and provide a comprehensive picture.

Conflicts of interest

There are no conflicts to declare.

Acknowledgements

This work was supported by the Institute for Basic Science (IBS-R004). We thank Junbeom Jo, Sungjun Park, Kyung Hwan Kim, Tokushi Sato, Ryo Fukaya, Kohei Ichiyanagi, and the beamline staff for the experiments performed at the BL3 of SACLA with the approval of the Japan Synchrotron Radiation Research Institute (proposal no. 2015B8054).

Notes and references

1 J. Franck and E. Rabinowitsch, *Trans. Faraday Soc.*, 1934, **30**, 120–130.
2 S. J. Harris, D. Murdock, Y. Zhang, T. A. Oliver, M. P. Grubb, A. J. Orr-Ewing, G. M. Greetham, I. P. Clark, M. Towrie, S. E. Bradforth and M. N. Ashfold, *Phys. Chem. Chem. Phys.*, 2013, **15**, 6567–6582.
3 I. A. Heisler and S. R. Meech, *Science*, 2010, **327**, 857–860.
4 J. A. Kloepfer, V. H. Vilchiz, V. A. Lenchenkov and S. E. Bradforth, *Chem. Phys. Lett.*, 1998, **298**, 120–128.
5 D. A. Braden, E. E. Parrack and D. R. Tyler, *Coord. Chem. Rev.*, 2001, **211**, 279–294.
6 N. Huse, B. Bruner, M. Cowan, J. Dreyer, E. Nibbering, R. Miller and T. Elsaesser, *Phys. Rev. Lett.*, 2005, **95**, 147402.
7 K. H. Kim, J. H. Lee, J. Kim, S. Nozawa, T. Sato, A. Tomita, K. Ichiyanagi, H. Ki, J. Kim, S. Adachi and H. Ihee, *Phys. Rev. Lett.*, 2013, **110**, 165505.
8 F. Liu, N. Luehr, H. J. Kulik and T. J. Martinez, *J. Chem. Theory Comput.*, 2015, **11**, 3131–3144.
9 S. Karashima, Y.-i. Yamamoto and T. Suzuki, *J. Phys. Chem. Lett.*, 2019, **10**, 4499–4504.
10 J. N. Miller and J. K. McCusker, *Chem. Sci.*, 2020, **11**, 5191–5204.
11 C. Lee, C. H. Choi and T. Joo, *Phys. Chem. Chem. Phys.*, 2020, **22**, 1115–1121.
12 H. Shimizu, K. H. Park, H. Otani, S. Aoyagi, T. Nishinaga, Y. Aso, D. Kim and M. Iyoda, *Chem.–Eur. J.*, 2018, **24**, 3793–3801.
13 G. Maier and H. P. Reisenauer, *Angew. Chem., Int. Ed.*, 1986, **25**, 819–822.
14 X. Zheng and D. L. Phillips, *Chem. Phys. Lett.*, 2000, **324**, 175–182.
15 M. Wall, A. N. Tarnovsky, T. Pascher, V. Sundström and E. Åkesson, *J. Phys. Chem. A*, 2003, **107**, 211–217.
16 C. P. Anderson, K. G. Spears, K. R. Wilson and R. J. Sension, *J. Chem. Phys.*, 2013, **139**, 194307.
17 K.-C. Tang, J. Peng, K. G. Spears and R. J. Sension, *J. Chem. Phys.*, 2010, **132**, 141102.
18 P. Y. Cheng, D. Zhong and A. H. Zewail, *Chem. Phys. Lett.*, 1995, **237**, 399–405.
19 V. A. Borin, S. M. Matveev, D. S. Budkina, P. Z. El-Khoury and A. N. Tarnovsky, *Phys. Chem. Chem. Phys.*, 2016, **18**, 28883–28892.
20 J. Yang, X. Zhu, T. J. A. Wolf, Z. Li, J. P. F. Nunes, R. Coffee, J. P. Cryan, M. Gühr, K. Hegazy, T. F. Heinz, K. Jobe, R. Li, X. Shen, T. Veccione, S. Weathersby, K. J. Wilkin, C. Yoneda, Q. Zheng, T. J. Martinez, M. Centurion and X. Wang, *Science*, 2018, **361**, 64–67.
21 Y. Liu, S. L. Horton, J. Yang, J. P. F. Nunes, X. Shen, T. J. A. Wolf, R. Forbes, C. Cheng, B. Moore, M. Centurion, K. Hegazy, R. Li, M.-F. Lin, A. Stolow, P. Hockett, T. Rozgonyi, P. Marquetand, X. Wang and T. Weinacht, *Phys. Rev. X*, 2020, **10**, 021016.
22 A. N. Tarnovsky, J. L. Alvarez, A. P. Yartsev, V. Sundstrom and E. Akesson, *Chem. Phys. Lett.*, 1999, **312**, 121–130.
23 A. N. Tarnovsky, V. Sundstrom, E. Akesson and T. Pascher, *J. Phys. Chem. A*, 2004, **108**, 237–249.
24 K. Saitow, Y. Naitoh, K. Tominaga and K. Yoshihara, *Chem.–Asian J.*, 2008, **3**, 696–709.
25 W. M. Kwok, C. S. Ma, A. W. Parker, D. Phillips, M. Towrie, P. Matousek and D. L. Phillips, *J. Chem. Phys.*, 2000, **113**, 7471–7478.
26 X. M. Zheng and D. L. Phillips, *J. Phys. Chem. A*, 2000, **104**, 6880–6886.
27 Y. L. Li, D. Q. Wang, K. H. Leung and D. L. Phillips, *J. Phys. Chem. A*, 2002, **106**, 3463–3468.
28 X. Guan, X. Lin, W. M. Kwok, Y. Du, Y. L. Li, C. Zhao, D. Wang and D. L. Phillips, *J. Phys. Chem. A*, 2005, **109**, 1247–1256.

29 J. Davidsson, J. Poulsen, M. Cammarata, P. Georgiou, R. Wouts, G. Katona, F. Jacobson, A. Plech, M. Wulff, G. Nyman and R. Neutze, *Phys. Rev. Lett.*, 2005, **94**, 245503.
30 J. Vincent, M. Andersson, M. Eklund, A. B. Wohri, M. Odelius, E. Malmerberg, Q. Y. Kong, M. Wulff, R. Neutze and J. Davidsson, *J. Chem. Phys.*, 2009, **130**, 154502.
31 S. Park, J. Choi, H. Ki, K. H. Kim, K. Y. Oang, H. Roh, J. Kim, S. Nozawa, T. Sato, S. I. Adachi, J. Kim and H. Ihee, *J. Chem. Phys.*, 2019, **150**, 224201.
32 M. N. Glukhovtsev and R. D. Bach, *Chem. Phys. Lett.*, 1997, **269**, 145–150.
33 D. L. Phillips and W.-H. Fang, *J. Org. Chem.*, 2001, **66**, 5890–5896.
34 M. Odelius, M. Kadi, J. Davidsson and A. N. Tarnovsky, *J. Chem. Phys.*, 2004, **121**, 2208–2214.
35 M. Kawasaki, S. J. Lee and R. Bersohn, *J. Chem. Phys.*, 1975, **63**, 809–814.
36 P. M. Kroger, P. C. Demou and S. J. Riley, *J. Chem. Phys.*, 1976, **65**, 1823–1834.
37 U. Marvet, Q. Zhang, E. J. Brown and M. Dantus, *J. Chem. Phys.*, 1998, **109**, 4415–4427.
38 B. J. Schwartz, J. C. King, J. Z. Zhang and C. B. Harris, *Chem. Phys. Lett.*, 1993, **203**, 503–508.
39 K.-i. Saitow, Y. Naitoh, K. Tominaga and K. Yoshihara, *Chem. Phys. Lett.*, 1996, **262**, 621–626.
40 D. Rimmerman, D. Leshchev, D. J. Hsu, J. Hong, I. Kosheleva and L. X. Chen, *J. Phys. Chem. Lett.*, 2017, **8**, 4413–4418.
41 J. M. Budarz, M. P. Minitti, D. V. Cofer-Shabica, B. Stankus, A. Kirrander, J. B. Hastings and P. M. Weber, *J. Phys. B: At., Mol. Opt. Phys.*, 2016, **49**, 034001.
42 T. C. Rossi, D. Grolimund, M. Nachtegaal, O. Cannelli, G. F. Mancini, C. Bacellar, D. Kinschel, J. R. Rouxel, N. Ohannessian, D. Pergolesi, T. Lippert and M. Chergui, *Phys. Rev. B: Condens. Matter Mater. Phys.*, 2019, **100**, 245207.
43 T. Ishikawa, H. Aoyagi, T. Asaka, Y. Asano, N. Azumi, T. Bizen, H. Ego, K. Fukami, T. Fukui, Y. Furukawa, S. Goto, H. Hanaki, T. Hara, T. Hasegawa, T. Hatsui, A. Higashiya, T. Hirono, N. Hosoda, M. Ishii, T. Inagaki, Y. Inubushi, T. Itoga, Y. Joti, M. Kago, T. Kameshima, H. Kimura, Y. Kirihara, A. Kiyomichi, T. Kobayashi, C. Kondo, T. Kudo, H. Maesaka, X. M. Maréchal, T. Masuda, S. Matsubara, T. Matsumoto, T. Matsushita, S. Matsui, M. Nagasono, N. Nariyama, H. Ohashi, T. Ohata, T. Ohshima, S. Ono, Y. Otake, C. Saji, T. Sakurai, T. Sato, K. Sawada, T. Seike, K. Shirasawa, T. Sugimoto, S. Suzuki, S. Takahashi, H. Takebe, K. Takeshita, K. Tamasaku, H. Tanaka, R. Tanaka, T. Tanaka, T. Togashi, K. Togawa, A. Tokuhisa, H. Tomizawa, K. Tono, S. Wu, M. Yabashi, M. Yamaga, A. Yamashita, K. Yanagida, C. Zhang, T. Shintake, H. Kitamura and N. Kumagai, *Nat. Photonics*, 2012, **6**, 540–544.
44 T. Katayama, Y. Inubushi, Y. Obara, T. Sato, T. Togashi, K. Tono, T. Hatsui, T. Kameshima, A. Bhattacharya, Y. Ogi, N. Kurahashi, K. Misawa, T. Suzuki and M. Yabashi, *Appl. Phys. Lett.*, 2013, **103**, 131105.
45 M. L. Shelby, P. J. Lestrange, N. E. Jackson, K. Haldrup, M. W. Mara, A. B. Stickrath, D. L. Zhu, H. T. Lemke, M. Chollet, B. M. Hoffman, X. S. Li and L. X. Chen, *J. Am. Chem. Soc.*, 2016, **138**, 8752–8764.
46 M. C. Langner, S. Roy, S. W. Huang, J. D. Koralek, Y. D. Chuang, G. L. Dakovski, J. J. Turner, J. S. Robinson, R. N. Coffee, M. P. Minitti, S. Seki, Y. Tokura and R. W. Schoenlein, *Phys. Rev. Lett.*, 2017, **119**, 107204.
47 Y. Obara, H. Ito, T. Ito, N. Kurahashi, S. Thurmer, H. Tanaka, T. Katayama, T. Togashi, S. Owada, Y. Yamamoto, S. Karashima, J. Nishitani, M. Yabashi, T. Suzuki and K. Misawa, *Struct. Dyn.*, 2017, **4**, 044033.
48 P. Wernet, *Philos. Trans. R. Soc., A*, 2019, **377**, 20170464.
49 K. H. Kim, J. G. Kim, S. Nozawa, T. Sato, K. Y. Oang, T. W. Kim, H. Ki, J. Jo, S. Park, C. Song, T. Sato, K. Ogawa, T. Togashi, K. Tono, M. Yabashi, T. Ishikawa, J. Kim, R. Ryoo, J. Kim, H. Ihee and S.-i. Adachi, *Nature*, 2015, **518**, 385–389.
50 E. Biasin, T. B. van Driel, K. S. Kjaer, A. O. Dohn, M. Christensen, T. Harlang, P. Chabera, Y. Z. Liu, J. Uhlig, M. Papai, Z. Nemeth, R. Hartsock, W. Liang, J. X. Zhang, R. Alonso-Mori, M. Chollet, J. M. Glownia, S. Nelson, D. Sokaras, T. A. Assefa, A. Britz, A. Galler, W. Gawelda, C. Bressler, K. J. Gaffney, H. T. Lemke, K. B. Moller, M. M. Nielsen, V. Sundstrom, G. Vanko, K. Warnmark, S. E. Canton and K. Haldrup, *Phys. Rev. Lett.*, 2016, **117**, 013002.
51 E. Biasin, T. Van Driel, G. Levi, M. Laursen, A. Dohn, A. Molkte, P. Vester, F. Hansen, K. Kjær, T. Harlang, R. Hartsock, M. Christensen, K. Gaffney, N. Henriksen, K. Møller, K. Haldrup and M. Nielsen, *J. Synchrotron Radiat.*, 2018, **25**, 306–315.
52 K. Haldrup, G. Levi, E. Biasin, P. Vester, M. G. Laursen, F. Beyer, K. S. Kjær, T. Brandt van Driel, T. Harlang, A. O. Dohn, R. J. Hartsock, S. Nelson, J. M. Glownia, H. T. Lemke, M. Christensen, K. J. Gaffney, N. E. Henriksen, K. B. Møller and M. M. Nielsen, *Phys. Rev. Lett.*, 2019, **122**, 063001.
53 K. S. Kjær, T. B. Van Driel, T. C. B. Harlang, K. Kunnus, E. Biasin, K. Ledbetter, R. W. Hartsock, M. E. Reinhard, S. Koroidov, L. Li, M. G. Laursen, F. B. Hansen, P. Vester, M. Christensen, K. Haldrup, M. M. Nielsen, A. O. Dohn, M. I. Pápai, K. B. Møller, P. Chabera, Y. Liu, H. Tatsuno, C. Timm, M. Jarenmark, J. Uhlig, V. Sundström, K. Wärnmark, P. Persson, Z. Németh, D. S. Szemes, É. Bajnóczi, G. Vankó, R. Alonso-Mori, J. M. Glownia, S. Nelson, M. Sikorski, D. Sokaras, S. E. Canton, H. T. Lemke and K. J. Gaffney, *Chem. Sci.*, 2019, **10**, 5749–5760.
54 B. Stankus, H. Yong, N. Zotev, J. M. Ruddock, D. Bellshaw, T. J. Lane, M. Liang, S. Boutet, S. Carbajo, J. S. Robinson, W. Du, N. Goff, Y. Chang, J. E. Koglin, M. P. Minitti, A. Kirrander and P. M. Weber, *Nat. Chem.*, 2019, **11**, 716–721.
55 K. Kunnus, M. Vacher, T. C. B. Harlang, K. S. Kjaer, K. Haldrup, E. Biasin, T. B. van Driel, M. Papai, P. Chabera, Y. Z. Liu, H. Tatsuno, C. Timm, E. Kallman, M. Delcey, R. W. Hartsock, M. E. Reinhard, S. Koroidov,

M. G. Laursen, F. B. Hansen, P. Vester, M. Christensen, L. Sandberg, Z. Nemeth, D. S. Szemes, E. Bajnoczi, R. Alonso-Mori, J. M. Glownia, S. Nelson, M. Sikorski, D. Sokaras, H. T. Lemke, S. Canton, K. B. Moller, M. M. Nielsen, G. Vank, K. Warnmark, V. Sundstrom, P. Persson, M. Lundberg, J. Uhlig and K. J. Gaffney, *Nat. Commun.*, 2020, **11**, 634.

56 J. G. Kim, S. Nozawa, H. Kim, E. H. Choi, T. Sato, T. W. Kim, K. H. Kim, H. Ki, J. Kim, M. Choi, Y. Lee, J. Heo, K. Y. Oang, K. Ichiyanagi, R. Fukaya, J. H. Lee, J. Park, I. Eom, S. H. Chun, S. Kim, M. Kim, T. Katayama, T. Togashi, S. Owada, M. Yabashi, S. J. Lee, S. Lee, C. W. Ahn, D.-S. Ahn, J. Moon, S. Choi, J. Kim, T. Joo, J. Kim, S.-i. Adachi and H. Ihee, *Nature*, 2020, **582**, 520–524.

57 I. Hargittai and M. Hargittai, *Stereochemical applications of gas-phase electron diffraction/Part A: the electron diffraction Technique*, VCH, Weinheim, 1988.

58 H. Yong, J. M. Ruddock, B. Stankus, L. Ma, W. Du, N. Goff, Y. Chang, N. Zotev, D. Bellshaw, S. Boutet, S. Carbajo, J. E. Koglin, M. Liang, J. S. Robinson, A. Kirrander, M. P. Minitti and P. M. Weber, *J. Chem. Phys.*, 2019, **151**, 084301.

59 H. Sakane, T. Mitsui, H. Tanida and I. Watanabe, *J. Synchrotron Radiat.*, 2001, **8**, 674–676.